Petroleum Science 21 (2024) 885–902

Contents lists available at ScienceDirect

Petroleum Science

journal homepage: www.keaipublishing.com/en/journals/petroleum-science

Original Paper

An adaptive physics-informed deep learning method for pore pressure prediction using seismic data

Xin Zhang [a, b], Yun-Hu Lu [a, b, c, *], Yan Jin [a, b, c], Mian Chen [a, b], Bo Zhou [d]

[a] State Key Laboratory of Petroleum Resources and Prospecting, China University of Petroleum (Beijing), Beijing, 102249, China
[b] College of Petroleum Engineering, China University of Petroleum (Beijing), Beijing, 102249, China
[c] College of Artificial Intelligence, China University of Petroleum (Beijing), Beijing, 102249, China
[d] PetroChina Tarim Oilfield Company, Korla, Xinjiang, 841000, China

ARTICLE INFO

Article history:
Received 12 April 2023
Received in revised form
11 October 2023
Accepted 6 November 2023
Available online 19 November 2023

Edited by Jie Hao and Meng-Jiao Zhou

Keywords:
Pore pressure prediction
Seismic data
1D convolution pyramid pooling
Adaptive physics-informed loss function
High generalization capability

ABSTRACT

Accurate prediction of formation pore pressure is essential to predict fluid flow and manage hydrocarbon production in petroleum engineering. Recent deep learning technique has been receiving more interest due to the great potential to deal with pore pressure prediction. However, most of the traditional deep learning models are less efficient to address generalization problems. To fill this technical gap, in this work, we developed a new adaptive physics-informed deep learning model with high generalization capability to predict pore pressure values directly from seismic data. Specifically, the new model, named CGP-NN, consists of a novel parametric features extraction approach (1DCPP), a stacked multilayer gated recurrent model (multilayer GRU), and an adaptive physics-informed loss function. Through machine training, the developed model can automatically select the optimal physical model to constrain the results for each pore pressure prediction. The CGP-NN model has the best generalization when the physics-related metric $\lambda = 0.5$. A hybrid approach combining Eaton and Bowers methods is also proposed to build machine-learnable labels for solving the problem of few labels. To validate the developed model and methodology, a case study on a complex reservoir in Tarim Basin was further performed to demonstrate the high accuracy on the pore pressure prediction of new wells along with the strong generalization ability. The adaptive physics-informed deep learning approach presented here has potential application in the prediction of pore pressures coupled with multiple genesis mechanisms using seismic data.

1. Introduction

Formation pore pressure is one of the most important reservoir parameters during hydrocarbon exploration and development, and it is critical for the analysis of multiphase fluid flow behaviors, well stability, and rational design of drilling plans (Agrawal et al., 2011; Dutta, 2002; Zhang, 2011). Accurate prediction of formation pore pressure can help optimize well structure design, improve mechanical drilling speed, maintain reservoir integrity, and subsequently enhance oil/gas recovery and production efficiency (Najibi et al., 2017; Opara and Onuoha, 2009). Besides, the accurate prediction of pore pressure values is also in favor of de-risking drilling accidents and reducing operation costs.

Conventional methods to predict pore pressure are usually developed based on physical models. Hottmann and Johnson (1965) were probably the first researchers to apply numerical methods to predict pore pressures. They proposed a method to estimate pore pressure directly using intersection plates based on the geology and drilling experience in Miocene and Oligocene shales in Upper Texas and Southern Louisiana Gulf Coast. Their results showed that the porosity and the sonic transit time became smaller with depth. The values conforming to the normal trend line were hydrostatic pressures, while the anomalous values deviating from the normal trend line were abnormal pore pressures. By studying the functional relationship between the pore pressure and the anomalous values, the intersection plot was then established. This intersection plate can directly read out the pore pressure at a certain depth. However, this method is purely empirical and is only suitable for a specific area (Zhang, 2011). Most commonly, the Eaton method (Eaton, 1975) based on the mechanism of under-

* Corresponding author.
E-mail address: luyh@cup.edu.cn (Y.-H. Lu).

https://doi.org/10.1016/j.petsci.2023.11.006

compaction has been widely applied for predicting formation pore pressure (Keshavarzi and Jahanbakhshi, 2013; Zhang, 2011; Zhang and Yin, 2017). The Eaton method is an effective stress method that establishes a relationship between the sonic transit time, resistivity, and pore pressure (Bowers, 1995). It usually requires the establishment of a normal compaction trend line. In the original Eaton equation, it is difficult to determine the normal shale resistivity under hydrostatic pore pressure conditions (Bowers, 1995; Zhang, 2011). Zhang proposed a fast method to calculate the compaction trend based on the relationship between the measured resistivity and the burial depth of the formation at normal pressure (Zhang, 2011). Based on the Eaton method, Bowers considered that the causes of anomalous high pressure were mainly under compaction and fluid expansion, and he proposed a loading model and an unloading model for these two mechanisms, respectively (Bowers, 1995, 2001). The method has been proved and applied well in high-pressure areas such as the Gulf of Mexico and the North Sea.

Besides, other methods such as Bayesian statistics (Oughton et al., 2018; Zhang et al., 2022), inversion method of geophysical anisotropic elastic parameter (Chen et al., 2023; Chen and Zong, 2022), and layer velocities interpreted from seismic data (Boer et al., 2006; Dutta, 2002) are also developed for pore pressure forecast. More methods have been proposed recently (Wessling et al., 2013; Yu et al., 2014; Gao et al., 2021; Zhang, 2011; Zhang and Yin, 2017; Gutierrez et al., 2006; Lopez et al., 2004), and they are extremely helpful in improving the accuracy of pore pressure prediction. However, the integrated model based on various petrophysical data still faces some challenges: (1) the establishment of normal trend lines and the determination of constant coefficients are highly influenced by human factors with great uncertainty (Bowers, 1995; Eaton, 1975); (2) a single model may be applicable only to a single formation, but is not suitable for pore pressure prediction in complex formations (Wang and Wang, 2015); (3) high-precision prediction methods for predicting pore pressure directly from high-dimensional data (e.g., seismic data) before drilling are still relatively scarce (Opara and Onuoha, 2009; Sayers et al., 2002).

Recently, the success of deep machine learning in a broad aspect of science and engineering topics (LeCun et al., 2015; Oprea et al., 2022; Jin et al., 2022; Ye et al., 2022) has shown its great potential in petroleum industry on the prediction of pore pressure. Weinzierl and Wiese (2021) used multidimensional rock physical properties for machine learning training to predict pore pressure. Huang et al. (2022) calculated pore pressure after machine training of logging and drilling parameters to predict effective stress and compared the prediction results of machine learning methods such as random forest, support vector machines, and multilayer perceptron neural networks. Matinkia et al. (2022) used an optimized deep learning model trained on log data to predict formation pore pressure and compared the prediction results with previous traditional physical methods. An increasing number of researchers are using machine learning methods to find nonlinear mapping relationships between real drilling and logging parameters and anomalous pore pressures (Farsi et al., 2021; Matinkia et al., 2022; Li et al., 2023). These studies have led to great success in the application of machine learning to pore pressure prediction.

However, the direct application of higher dimensional data such as seismic data to the pore pressure prediction problem is still quite challenging, especially in making it highly generalizable. Moreover, literature review indicates that most of the studies focus on sandstone and shale formations, with less research on pore pressure in carbonate rocks. It also shows more focus on real drilling and logging parameters, and less research on machine learning methods to predict pore pressure from seismic data. However, pre-drill pore pressure prediction is often very important. Considering the complexity of pore pressure prediction in carbonate rocks, machine learning methods have significant advantages in complex nonlinear modeling, and thus it is of great significance to study its application. This research proposes a machine learning method for direct prediction of pore pressure from seismic data under physical model constraints based on carbonate rock data from the Tarim Basin.

The main structure of the work is organized as follows: We first introduce the adaptive physics-informed deep learning model in Section 2. The new 1D convolution pyramid pooling (1DCPP) model, a multilayer GRU neural network and an adaptive physics-informed constraint method will be described in detail. Methods for evaluating the performance of prediction results are also introduced. The associated seismic attribute data and pore pressure prediction workflow are described in Section 3. Section 4 presents the result and discussion, including data pre-processing, physical regularization optimization, comparison of test results, regional pressure distribution, and some shortcomings. Finally, the conclusions are presented, and more data details are provided in Appendix A and B.

2. Physics-informed deep learning model

In this work, we present a physics-informed deep learning model named CGP-NN. As shown in Fig. 1, CGP-NN contains a new 1DCPP model, a multilayer GRU neural network and a new adaptive physics-informed constraint method.

First, in the 1DCPP model, 1D convolution focus on extracting the features of the high-dimensional parameters. Then, the features are transformed into a vector feature by the pyramid pooling technique. Finally, a multilayer GRU network concentrates on prediction of pore pressure. During the training process of the multilayer GRU, the adaptive physics-informed constraint method automatically selects the most appropriate physical model as a constraint based on the error variation among the predicted values, the calculated values of the physical model and labeled values. In the following, we describe the CGP-NN model in detail.

2.1. 1DCPP model

Previous studies (Dong et al., 2016; Huang et al., 2017; Matinkia et al., 2022; Li et al., 2023; Szegedy et al., 2015) have proved that CNN is capable of effectively extracting important features of parameters, and integrating from shallow local features to obtain deeper high-dimensional features. Different CNN models have nearly identical characteristics and processing methods, with the key difference being the dimensionality of the input data and how the convolution kernel slides through the data. The 1D-CNN model can achieve feature extraction and regression analysis of samples directly by adjusting the convolutional kernel size and shift direction compared to the other models. Therefore, the 1D-CNN model is capable of avoiding the complex operations required to construct and process multidimensional samples.

Classical CNN models use multiple fully connected layers after the convolutional layers, which leads to a dramatic increase in the number of trainable parameters, the amount of computer computation and the required storage space. In this work, the pyramid pooling method (He et al., 2015) is adopted to solve this problem, which helps avoid the repeated computation of the convolutional features. We define a new network structure with a pyramid pooling layer, which can extract the maximum value from a certain direction along a fixed window range for the parameter features given by the earlier convolutional layers. The pyramid pooling operation is an extension of the maximum pooling operation. Unlike traditional maximum pooling layers, the same set of

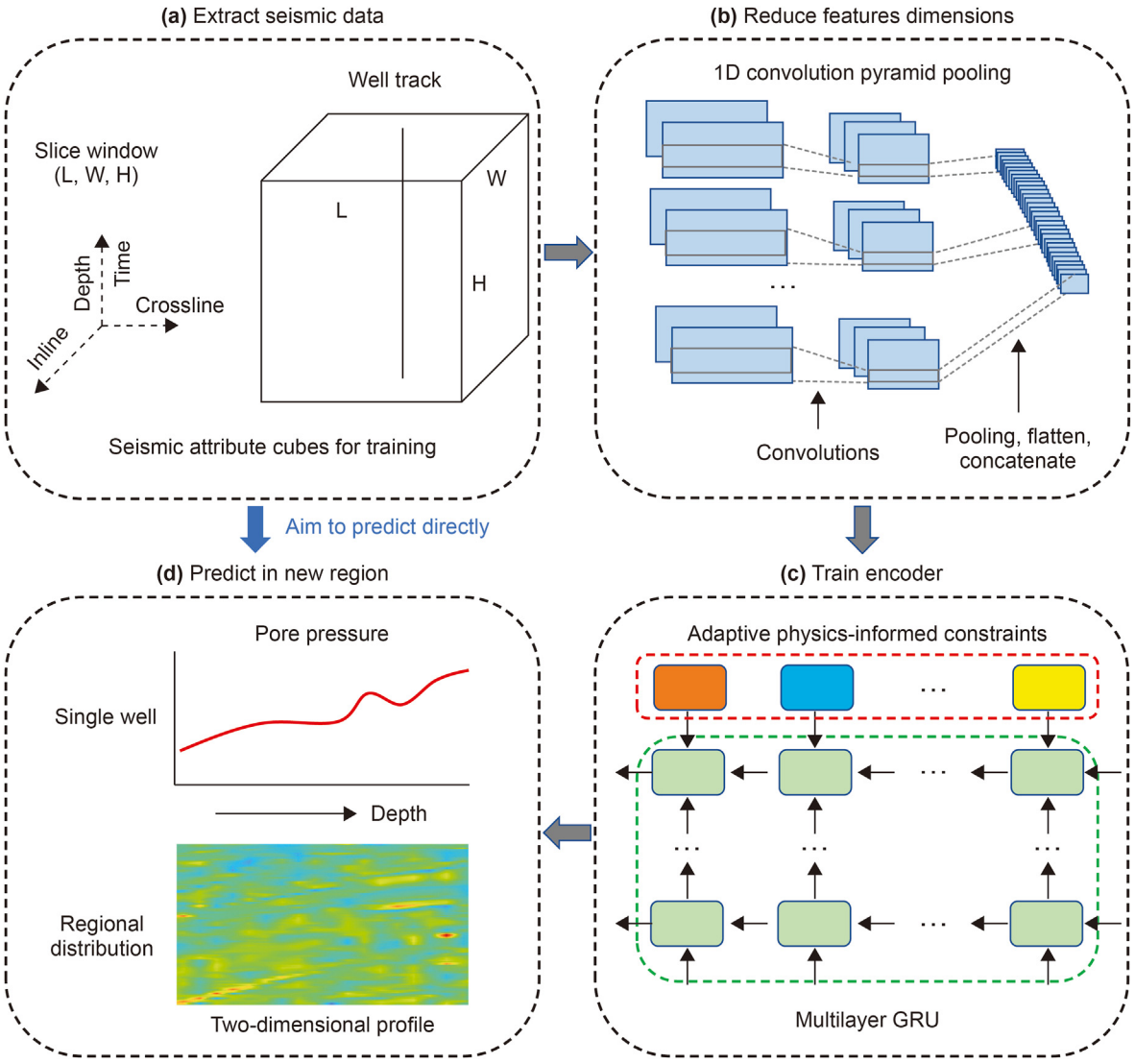

Fig. 1. Framework of the CGP-NN model.

convolutional feature parameters can be pooled multiple times by pyramid pooling. The feature parameters of the 1DCPP structure is generated from a window of input data, which can be described by the following equations:

$$c_k = f(w \cdot x_{k:k+h-1} + b) \tag{1}$$

$$c = [c_1, c_2, \cdots, c_{n-h+1}] \tag{2}$$

$$\hat{c}' = [\max\{c_1, c_2, \cdots, c_m\}, \max\{c_m, c_{m+1}, \cdots, c_{2m}\}, \cdots,] \tag{3}$$

$$\hat{c}'' = [\max\{c_1, c_2, \cdots, c_p\}, \max\{c_p, c_{p+1}, \cdots, c_{2p}\}, \cdots,] \tag{4}$$

$$\hat{c} = \hat{c}' \oplus \hat{c}'' \oplus, \cdots, \oplus \hat{c}''' \cdots \tag{5}$$

where $x_{k:k+h-1}$ is the concatenation of the input data x_k, x_{k+1}, $\cdots, x_{k+h-1}$; w, h, b are a filter, a window, and a bias term, respectively; f is a non-linear function such as the hyperbolic tangent; c_k is a feature generated from a window of data $x_{k:k+h-1}$; c is a feature map generated from each window of data $\{x_{1:h}, x_{2:h+1}, \cdots, x_{n-h+1:n}\}$; $\hat{c}'$ is the first maximum pooling operation for c, based on the pool size m; $\hat{c}''$ is the second maximum pooling operation for c, based on the pool size p; $\hat{c}$ is the feature that concatenates $\hat{c}', \hat{c}'', \cdots, \hat{c}''' \cdots$; $\oplus$ is the concatenation operator.

The schematic diagram of the 1DCPP model is illustrated in Fig. 2, which contains three 1DCPP structures. In this convolution pyramid pooling structure, the data matrix of 8*5 uses a convolution operation: 3 filters, 3 kernels and 1 stride, where the filters represent the number of parametric features to be extracted, kernel is the window size of the filter, and stride is the magnitude of each filter shift, respectively. The result of the convolution operation of each filter will generate 1 feature vector after the action of the activation function. Therefore, 3 filters will generate 3 feature vectors with dimension 6*1. Then, pyramid pooling techniques of size 2*1 and 3*1 are used on these 3 feature vectors respectively. In this way, multiple sets of pooled vectors with different features are obtained. Finally, the data vector for training can be obtained by the flatten and concatenate operations. The 1DCPP model combines the advantages of 1DCNN (Kim, 2014; Zhao, 2019) and spatial pyramid pooling (He et al., 2015), which is capable of extracting parametric features from high-dimensional seismic data and thus enhancing

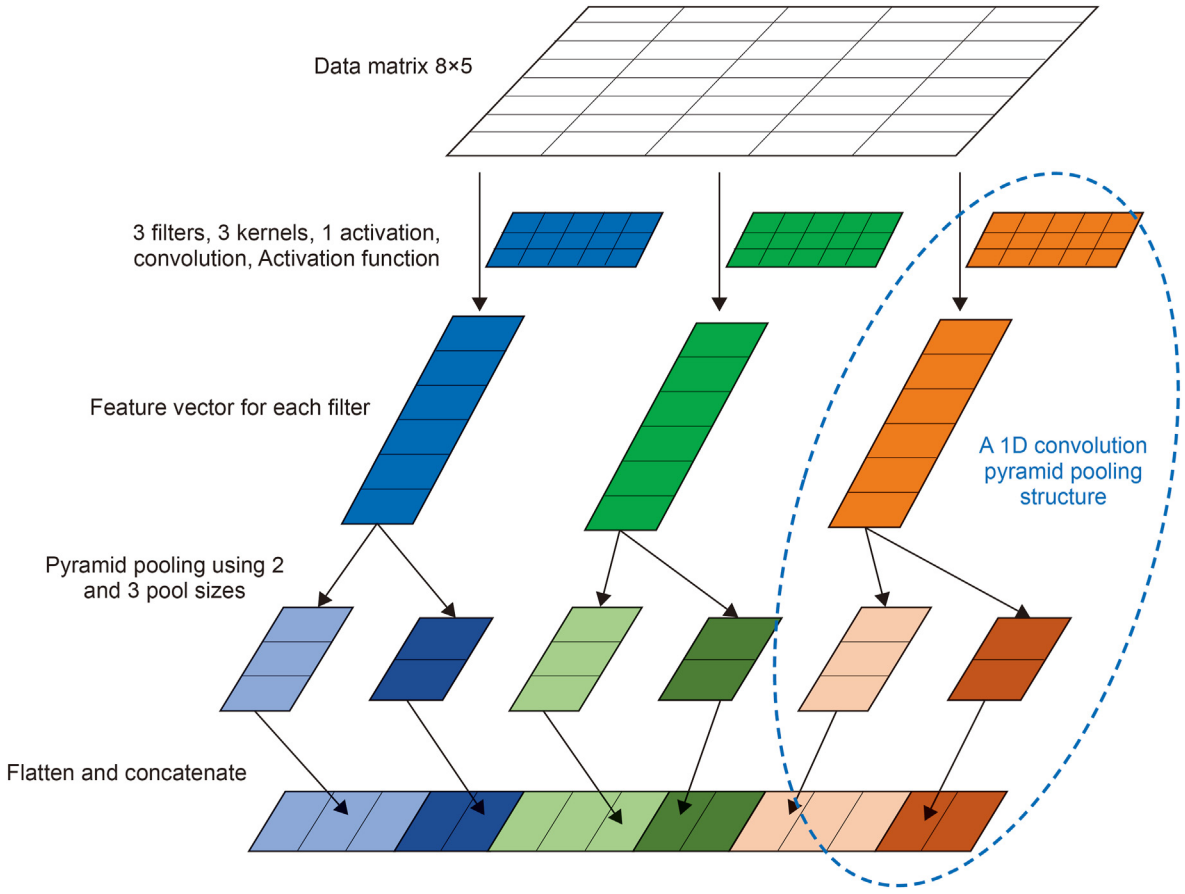

Fig. 2. The schematic diagram of a 1DCPP model (hyper-parameters: numbers of filters = 3, kernel size = 3, stride = 1, pool size = 2, 3).

the learning efficiency of the CGP-NN model as well as saving computational resources.

Moreover, a 1DCPP model can consist of multiple 1DCPP structures. Multiple combinations of kernels and strides can be achieved with different 1DCPP structures. In this case, it will be 3 structures in the 1DCPP model with 1 stride. Then the data features can be trained by multilayer GRU after connecting the data features through the concatenate layer and the pooling layer.

2.2. Multilayer GRU method

The depth-dependent pore pressure prediction problem can be considered as a typical time series problem, while the seismic data can be viewed as a set of multivariate time series sample data. GRU is capable of handling these forecasting problems (Cho et al., 2014; Chung et al., 2014). The training result of GRU is similar to the result of LSTM (Hochreiter and Schmidhuber, 1997), but it will greatly simplify computer operations. A basic GRU unit consists of an update gate and a reset gate, which can be described by the following equations:

$$z_t = \text{sigmoid}(W_z \cdot x_t + U_z \cdot h_{t-1}) \tag{6}$$

$$r_t = \text{sigmoid}(W_r \cdot x_t + U_r \cdot h_{t-1}) \tag{7}$$

$$\tilde{h}_t = \tanh(W \cdot x_t + U(r_t \odot h_{t-1})) \tag{8}$$

$$h_t = (1 - z_t) \cdot h_{t-1} + z_t \cdot \tilde{h}_t \tag{9}$$

where z_t is an update gate; r_t is a reset gate; $\tilde{h}_t$ is a candidate activation; h_t is the activation at time t; Sigmoid function is a function that ranges from 0 to 1; W_z, W_r, U_z, U_r are the weight parameters of each gate; x_t is the input value at time t; $h_{t\text{-}1}$ is the previous activation which is a hidden state at time t-1; the symbol $\odot$ is the Hadamard product, which is the multiplication of the corresponding entries in the operation matrix.

Fig. 3 shows a multilayer GRU model to predict the value of pore pressure. The parametric features of 1DCPP model are passed to the first GRU layer. Each layer of GRU receives the information from the previous adjacent layer, and the value of pore pressure can be predicted after the training of L-layer GRU. Usually, the GRU model can better extract nonlinear features as the number of layers increases. However, a GRU model with 2–4 layers is proposed to prevent overfitting problems and increased computer computation.

2.3. Adaptive physics-informed loss function

Loss function is used to evaluate the inconsistency between the predicted value of the model and the real value. Usually, it is a non-negative real-valued function shown as follows:

$$L_{\text{mse}} = \frac{1}{N}\sum_{i=1}^{N}\left(P^i_{\text{pred}} - P^i_{\text{actu}}\right)^2 \tag{10}$$

where L_{mse} is the mean-squared loss function; N is the number of

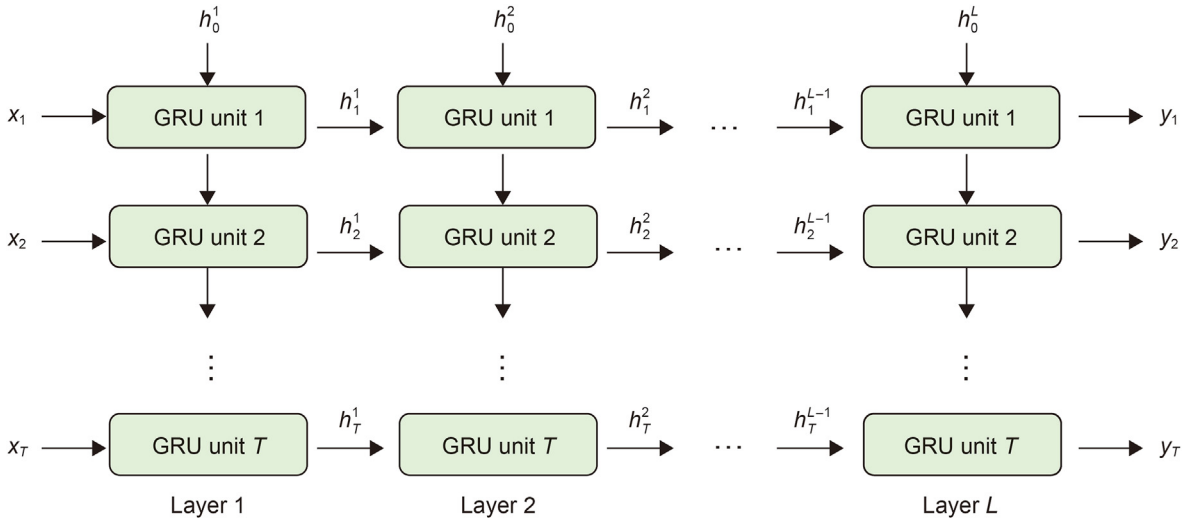

Fig. 3. The structure of multilayer GRU model.

samples; P^i_{pred}, P^i_{actu} are the predicted and actual values of the i-th sample respectively.

The robustness of the model will be better if the loss function is smaller. However, one of the problems is that the training process only seeks the minimum number loss value, leading to overfitting of the training data. Overfitting can lead to a decrease in the generalization ability of the model.

Physics-informed training method is an effective way to increase the generalization prediction performance of the training model. By using physics-informed training, the trainable parameters are penalized by a large update step if the predicted values are far from the corresponding physical metrics. This means that physics-informed training suppresses the overfitting problem of training data by providing a solution with physical constrains. The physics-informed loss function can be denoted by Eq. (11):

$$L_{\text{phy}} = \frac{1}{N}\sum_{i=1}^{N}\left(P^i_{\text{pred}} - P^i_{\text{phy}}\right)^2 \tag{11}$$

where L_{phy} is the physics-informed loss function; N is the number of samples; P^i_{pred}, P^i_{phy} are the predicted values and physics metrics of the i-th sample respectively. The minimum sum of the mean-squared loss and the physics-informed loss represents the most optimal model training result.

It is well known that different theoretical models are applicable to different stratigraphic conditions. However, no single theoretical model can be applied to meet all stratigraphic conditions. In this work, two theoretical methods of pore pressure prediction are used as adaptive physical regularities, namely Eaton method and Bowers method. The pore pressure obtained by Eaton method can be expressed as

$$P_{\text{eaton}} = \left[\rho_{\text{over}} - (\rho_{\text{over}} - \rho_w)\left(\frac{\Delta t_{\text{n}}}{\Delta t}\right)^n\right] gH \tag{12}$$

where ρ_{over} is the overburden stress gradient, g/cm^3; ρ_w is the hydrostatic pore pressure gradient, g/cm^3; Δt_{n} is the compressional transit time in shales at the normal pressure, us/ft; Δt is the compressional transit time obtained from the logs, μs/ft; n is the Eaton index, which usually sets to 3; g is the acceleration of gravity, m/s^2; H is the depth of the prediction point, m. The pore pressure predicted by Bowers method can be shown as

$$P_{\text{bowers}} = \sigma_{\text{v}} - \left(\frac{v_{\text{p}} - v_{\text{ml}}}{A}\right)^{\frac{1}{B}} \tag{13}$$

where σ_{v} is the overburden stress, MPa; v_{p} is the compressional velocity at the prediction point, km/s; v_{ml} is the compressional velocity in the ground surface, km/s; A, B are the experience coefficients of the study area.

Then, the adaptive physics-informed loss function of different pore pressure theoretical prediction methods (shown in Eq. (11)) can be written as Eq. (14):

$$L_{\text{phy}} = \frac{1}{N}\sum_{i=1}^{N}\left[\min\left(\left|P^i_{\text{pred}} - P^i_{\text{eaton}}\right|, \left|P^i_{\text{pred}} - P^i_{\text{bowers}}\right|\right)\right]^2 \tag{14}$$

where P^i_{eaton}, P^i_{bowers} are predicted values of the i-th sample by Eaton method and Bowers method, respectively. At each iteration of training, the adaptive physics-informed loss function will seek the closest prediction to one of the three theoretical pore pressure prediction methods by using the algorithm in Table 1. Finally, the adaptive physics-informed loss function can be described as

$$L_{\text{loss}} = \text{argmin}\left(L_{\text{mse}} + \lambda L_{\text{phy}}\right) \tag{15}$$

where λ is a hyperparameter representing physics-related metrics.

2.4. Evaluating prediction performance

The coefficient of determination (R^2) is used to evaluate the performance of the prediction results (Tjur, 2009), which can be expressed as Eq. (16):

$$R^2 = 1 - \frac{\sum_{i=1}^{M}\left(P_{\text{ture}} - P_{\text{pred}}\right)^2}{\sum_{i=1}^{M}\left(P_{\text{ture}} - P_{\text{mean}}\right)^2 + K.epsilon()} \tag{16}$$

where P_{ture}, P_{pred}, P_{mean} are the actual pore pressure values of the formation, the model prediction values, and the average of the actual pressure, respectively; M is the number of the samples;

Table 1
Algorithm of the adaptive physics-informed loss function.

Algorithm: the pseudocode of adaptive physics-informed loss function
Input: the predicted values P_{pred}, the physical model: P_{eaton}, P_{bowers} 1. Calculate the values of a, b, where $a = \left\|P^i_{pred} - P^i_{eaton}\right\|$, $b = \left\|P^i_{pred} - P^i_{bowers}\right\|$ 2. Retain the minimum value of a, b 3. Calculate the values of L_{loss} by using the minimum values 4. Until L_{loss} is smaller than the specified error 5. End training Output: the final prediction values

K.epsilon() is a very small value, and equal to 10^{-7}, in order to prevent the zero-denominator appearing. The coefficient of determination measures how well a statistical model predicts an outcome. The advantages of this method are that it is suitable for nonlinear correlation between variables, and its values can only range between 0 and 1. In other words, the closer the value of R^2 is to 1, the better the performance of the prediction model and the more accurate the prediction results.

3. Data and methodology

3.1. Seismic data

To investigate the validity of the CGP-NN approach, a complex reservoir in the Tarim Basin was used as a case study. Data of depth and 11 typical seismic attributes were selected as data inputs for the original machine learning model (Cibin, 1999; Subrahmanyam and Rao, 2008). The summary of these seismic attributes is shown in Table 2. Besides, the statistical description of different seismic attributes for machine learning is shown in Table 3. The seismic attributes have been converted to the depth domain data by a priori processing of drilled well constraints. The lithology of the studied strata is very complex, with several major sedimentary groups containing a variety of lithologies. The depth of wells in the working area reached more than 6000 m.

3.2. Well data

In the oil industry, using data from drilled wells as a constraint is a good strategy to better predict pore pressures when pre-drill prediction methods are used. As shown in Fig. 4, three ultra-deep straight wells (P1–P3) were used as training wells and the remaining one (P4) was used as a predictive test well. The target well can test the accuracy of the prediction results by comparing them with measured pore pressure values after training. Table 4 presents the measured pressure values of these wells.

3.3. Methodology

The workflow of pore pressure prediction methodology using seismic data is shown in Fig. 5. The key steps of the method are as follows:

Step 1. Gathered data. It is necessary to extract the well seismic track attribute data for deep learning. The summary of typical seismic attributes used for training and testing are shown in Table 2. In addition, the small number of pore pressure measurements, as shown in Table 4, do not directly serve as labels for machine learning. This research uses a hybrid approach that combines the advantages of Eaton and Bowers methods as learning labels. This will be explained in detail in section 4.1.

Step 2. Data processing. Different seismic attributes have different magnitudes and large differences in numerical magnitudes, which can seriously affect the machine learning prediction results. To eliminate these effects, normalization and parameterization of the data are necessary. Normalization and parameterization can speed up the training of the model and improve the prediction accuracy of the model.

Step 3. Training set, validation set, and test set. Rational division of data into training set, validation set and test set is effective to improve the generalization ability of prediction model. In this study, the data of well P4 is used as the test data, and then an equal amount of data is randomly selected from Wells P1–P3 as the validation data and the remaining data as the training data. The ratio of training set, verification set and test set is about 6.6:1.7:1.7, which is close to 6:2:2.

Step 4. Pore pressure prediction using machine learning. This CGP-NN model was used to predict the pore pressure. The 1DCPP method is used to extract data features, the multilayer GRU method is used for data training, and the adaptive physics-informed loss function is used for physical regularization optimization.

Step 5. Engineering application. After testing the model with P4 wells, this research generalized the prediction model to the entire study area. Section 4 will present a comparison of the

Table 2
Summary of typical seismic attributes used for machine learning.

No.	Attributes	Comment
1	Instantaneous frequency	Mean amplitude of the wavelet
2	Instantaneous Q	Related to attenuation
3	Maximum curvature	Maximum curvature of reflectors
4	Oriented filter	Related to the direction and angle
5	Reflection intensity	Distinguish between different lithologies
6	Relative acoustic impedance	Is an indicator of impedance changes, in a relative sense
7	RMS amplitude	Information about the energy content
8	Sampling point gradient	Reflection waveform
9	Spectral decomposition	Reflect the amplitude information of different frequency components
10	Time-lapse	Show continuity and discontinuity
11	Tomography focusing	Enhance fault texture

Table 3
Statistical description of different seismic attributes for machine learning.

Statistical index	Seismic attributes No.										
	1	2	3	4	5	6	7	8	9	10	11
Minimum	128.67	0.00	−3.37	−21,461.43	−2414.90	0.00	154.20	15.50	0.00	−21,468.00	−6559.60
Median	6455.31	1.22	0.00	−129.38	4.51	0.99	4082.76	162.00	95.00	−124.00	9.09
Mean	7523.17	1.13	−0.02	−9.54	3.19	2148.19	5142.51	183.28	104.38	−9.02	7.46
Maximum	21,569.02	1.57	0.75	19,896.60	3146.98	722,891.56	19,479.13	531.00	255.00	19,902.00	6807.88
Count	7188										

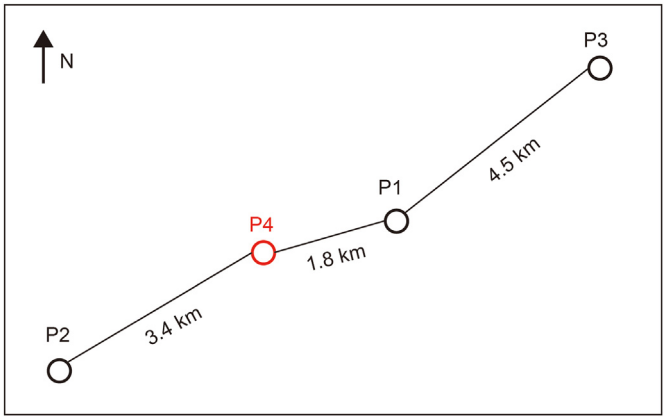

Fig. 4. Well relative location distribution. Seismic data from P1 to P3 are used for training, while P4 is used for predictive test.

generalization results. Moreover, with the promotion of engineering applications, it can continuously promote the improvement of CGP-NN model.

4. Results and discussion

4.1. Pre-processing

4.1.1. Label

Supervised machine learning methods require a large number of labels, and a small number of pore pressure measurement points cannot satisfy the training requirements for machine learning. Therefore, the measurement points need to be expanded into labels that can be used for machine learning. This study presents a hybrid approach that combines the Eaton and Bowers methods to establish machine-learnable labels. As shown in Fig. 6, the prediction results of the Eaton method are more accurate in the depth interval of 3000–4250 m, while the Bowers method is more accurate in the depth interval of 4250–5700 m. The hybrid approach is that these relatively accurate results are combined as the optimal prediction, which is more consistent with the actual measured points. Fig. 6 shows the labeling process for well P1, while the other wells are presented in Appendix A.

4.1.2. Normalization

Normalization can improve the stability of parameter features, which is helpful to improve the performance of machine learning. Seismic attributes are processed as input data by the minimum and maximum normalization approach as shown in equation:

$$X' = \frac{X - X_{\text{mean}}}{X_{\max} - X_{\min}} \tag{17}$$

where X' is the normalized value of the input data, and X_{mean}, $X_{\max}$, $X_{\min}$ correspond to the average, maximum and minimum values of the input data, respectively. Then the parametric features for CGP-NN model training are generated after PCA-based parameterization. The principal component of the PCA-based method is set to 0.95.

To obtain a prediction model with better generalization capability, the seismic data for training (P1–P3) are further divided into training and validation sets. The ratio of training set, verification set and test set is close to 6:2:2. When the training effect of both training and validation sets are high and close, we believe that the

Table 4
Measured pore pressure over well P1 to P4.

Well P1				Well P4			
Zone	Depth, m	pp, Psi	pp, MPa	Zone	Depth, m	pp, Psi	pp, MPa
N_{1j}	3518.06	7099.37	48.96	N_{1k}	2110	3802.612	26.2
N_{1j}	4249.31	10,205.48	70.38	N_{1-2k}	3160	6908.563	47.6
N_{1j}	4277.43	12,643.73	87.19	N_{1j}	3989	8751.814	60.3
N_{1j}	4883.68	14,435.76	99.55	N_{1j}	4609	11,248.19	77.5
E_{2-3s}	5346.18	15,043.11	103.74	N_{1j}	5109	12,830.19	88.4
$E_{1-2}km_1$	5564.93	15,421.38	106.35	N_{1j}	5329	14,034.83	96.7
$E_{1-2}km_2$	5630.56	14,322.97	98.77	E_{2-3s}	5454	13,062.41	90
$E_{1-2}km_3$	5889.93	15,652.39	107.94	$E_{1-2}km_1$	5598	15,457.18	106.5
$E_{1-2}km_4$	6039.93	12,617.64	87.01	$E_{1-2}km_2$	5807	12,336.72	85
K_1b_s	6074.31	16,573.98	114.29	–	–	–	–
Well P2				**Well P3**			
Zone	Depth, m	pp, Psi	pp, MPa	Zone	Depth, m	pp, Psi	pp, MPa
N_{1k}	2500	4644.412	32	N_{1j}	4800	13,134.98	90.5
N_{1-2k}	3518.057	7105.556	48.95728	–	–	–	–
N_{1j}	3914	11,320.75	78	–	–	–	–
N_{1j}	4277.432	12,654.74	87.19118	–	–	–	–
N_{1j}	4850	13,287.22	91.54898	–	–	–	–

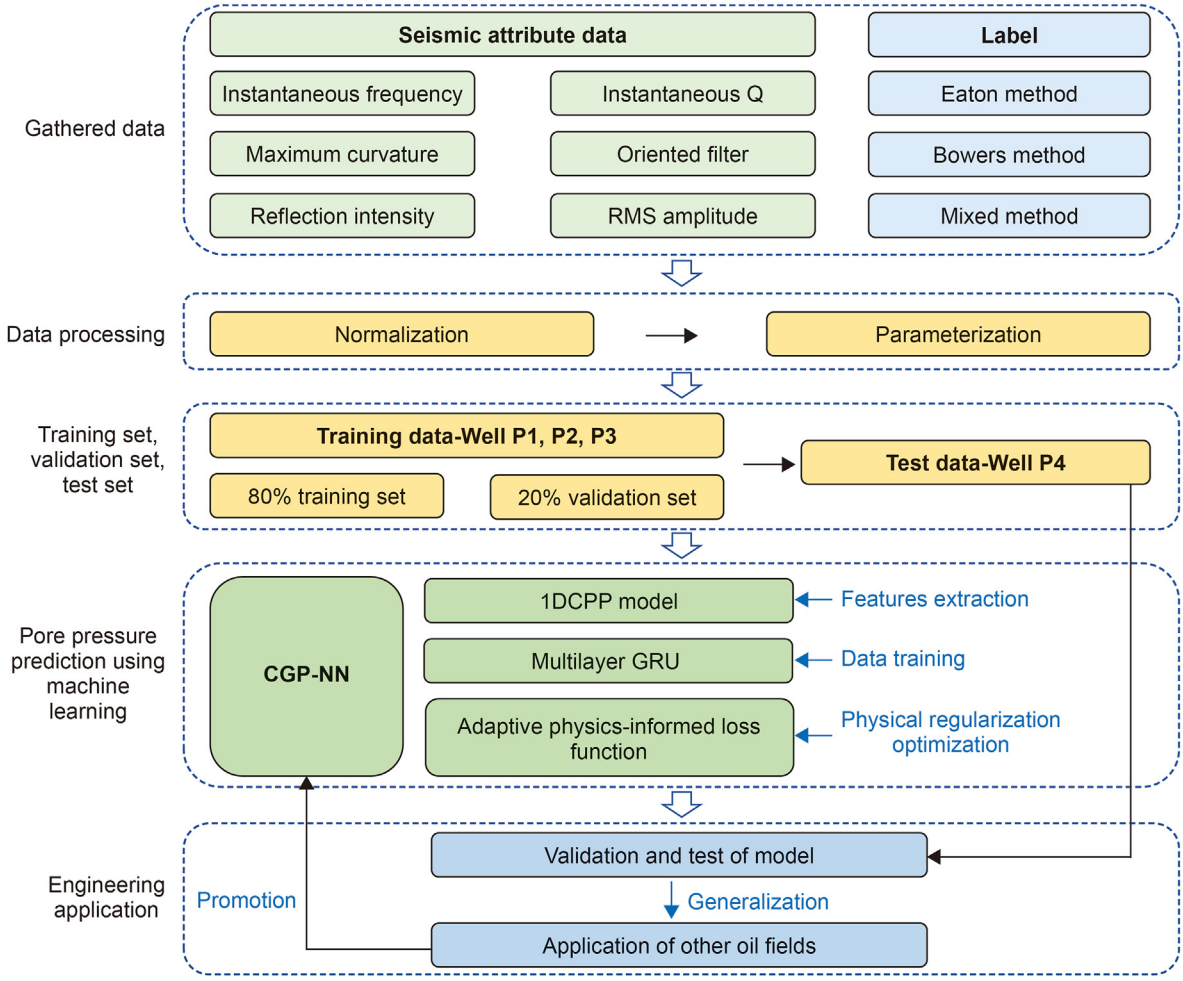

Fig. 5. Workflow of pore pressure prediction using seismic data.

acquired model has the strongest generalization ability and the best prediction efficiency.

4.1.3. Parameterization

PCA is a principal components analysis technique that converts multiple indicators into several composite indicators (Yang et al., 2004). This makes the data set of parametric features easier to train and reduces the computational cost. The algorithm of the PCA method is presented in Table 5 and the results of seismic attributes data after PCA are illustrated in Fig. 7.

4.2. Developing CGP-NN model

4.2.1. CGP-NN architecture

Fig. 8 details the CGP-NN architecture for this specific case study. In the structure of 1DCPP, multiple pooling operations are carried out on multiple parallel convolutional layers, and the concatenate layer is innovatively used to connect these pooling layers after the flatten operation. The parametric features of the 1DCPP model provide the information about the formation near the predicted point. In this work, we set the kernel window size to 2, 4, 8. And the data interval along the formation depth is 1 m. Therefore, the kernel window size 2, 4, 8 correspond to a formation depth of 4, 8, 16 m at the predicted points. Then the data features can be trained by multilayer GRU network for prediction of pore pressure. These hyper-parameters are set according to the data parameter characteristics, which are presented in Table 6. The total parameter numbers for the case study are 133,414.

4.2.2. Physics-informed regularization

To better demonstrate the advantages of the adaptive physical constraint model, we repeated training using different physical terms $\lambda(0,0.5,1)$. Additional $\lambda(0.2,0.4,0.6,0.8)$ training results are presented in Appendix B. λ is a hyperparameter representing physics-related metrics. The different values of λ represent the extent to which physical constraints are involved in machine learning. A value of zero means no physical constraint is engaged, while a value of one means that the degree of the constraint is at maximum.

Fig. 9 shows the prediction accuracy for each λ value. The training set with $\lambda = 0$ has the highest training accuracy of 0.99. However, the accuracy of the validation set is not high, which means the generalization ability of the model is very weak.

The training accuracy of the training set with $\lambda = 0.5$ is 0.97, but the accuracy of the validation set is also very high, indicating that this model is more ideal. It is worth noting that the model with $\lambda = 0.5$ achieves a high accuracy with a very short number of epochs, as shown in Fig. 9. This suggests that the physics-informed predictive model has an accelerating convergence effect.

It should also be noted that the training accuracy of both the training set and validation set with $\lambda = 1$ is low, although both prediction accuracies remain consistent. This is due to the excessive

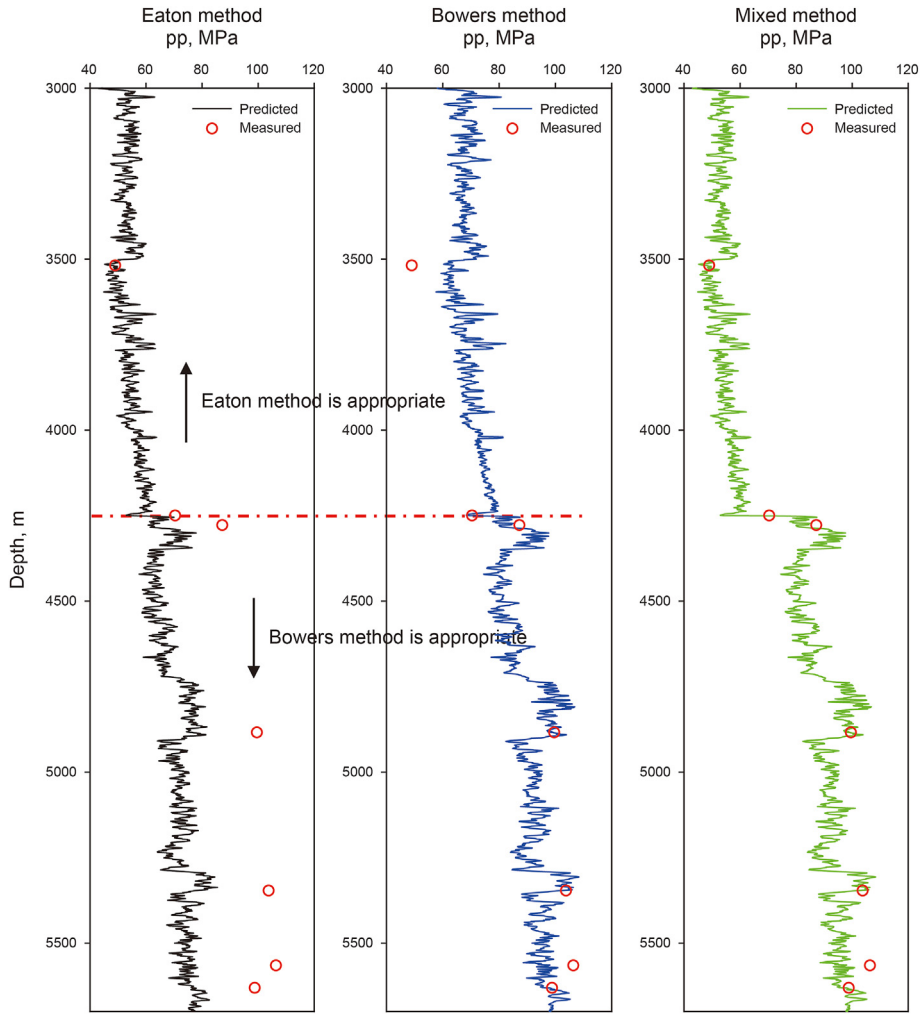

Fig. 6. Pore pressure labels for well P1.

Table 5
Algorithm of the PCA method.

Algorithm: the pseudocode of the PCA method
Input: the seismic data matrix: *m* rows, *n* columns 1. Transpose the seismic data matrix, called **X** 2. Zero-averaging each row of matrix **X** 3. Calculate the eigenvalues and eigenvectors of the covariance matrix of matrix **X** 4. Arrange the feature vectors in descending order of corresponding eigenvalue size 5. Take the first *K* rows as the matrix **P** 6. Multiply the matrix **P** with the matrix **X**, namely matrix **Y** Output: dimensionality reduction to K-dimensional matrix data: **Y**

involvement of physical constraints, leading to a reduction in the accuracy of the machine learning model. In other words, the prediction model is under-fitted because of the over-constraint of the physical criterion. Since the physical model can only represent part of the stratigraphic information, it is understood that over-constraint will stop the machine learning model from learning more information on the stratigraphic features.

Fig. 10 presents the loss values of training and validation sets with different λ. It is clear that the under fitting of $\lambda = 1$ leads to a large loss value compared to $\lambda = 0$ or $\lambda = 0.5$. Similarly, the gradual separation of the loss values from the training and validation sets for $\lambda = 0$ shows that this model is overfitting. However, for the ideal model, the loss values of the training and validation sets with $\lambda = 0.5$ are relatively small and very close.

4.3. Target well validation

The formation of target well P4 is very complex, consisting of a variety of lithologies including mudstone, sandstone, salt-gypsum rock and carbonate rock. The lithology of the formation in the well section 4000–4304 m and 4304–5300 m is mainly mudstone and salt-gypsum rock, respectively; the main composition of the well section 5300–5555 m is mudstone and salt-gypsum rock interbed; the well section 5555–6005 m is composed of mudstone, sandstone, salt-gypsum rock section and carbonate rock.

From the logging data shown in Fig. 11, a higher gamma content

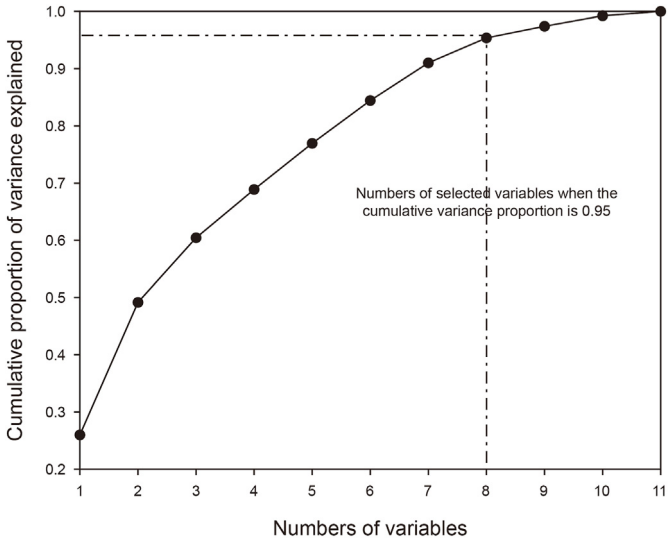

Fig. 7. Schematic diagram of the PCA method.

is observed at the well depth less than 4304 m. Meanwhile, the sonic transit time gradually decreases, indicating a higher fraction of mudstone and that the formation abnormal pore pressure mechanism is mainly consistent with the under-compaction mechanism. At the well depth greater than 4304 m, however, both gamma and sonic transit time curves fluctuate drastically, suggesting that the formation pore pressure is caused by complex and diverse mechanisms. This is in line with the observation of a large variation of the pore pressure values measured at this section. Therefore, the accurate prediction of pore pressure in this well from conventionally physical methods is very challenging.

The prediction results of well P4 as a test set using the optimal prediction model with $\lambda = 0.5$ are shown in Fig. 11. The correlation coefficient between the actual and predicted points of the new method reached 0.94, which was evaluated by Pearson's method. In particular, the prediction results were compared with those of the Eaton method, Bowers method, and CNN method. Correspondingly, the correlation coefficients of the corresponding methods were 0.85, 0.89, 0.9.

The Pearson's method can be expressed as the following equation:

$$r = \frac{\sum_{j}^{k}\left(P_j^{\text{pred}} - \overline{P^{\text{pred}}}\right)\left(P_j^{\text{actual}} - \overline{P^{\text{actual}}}\right)}{\sqrt{\sum_{j}^{k}\left(P_j^{\text{pred}} - \overline{P^{\text{pred}}}\right)^2}\sqrt{\sum_{j}^{k}\left(P_j^{\text{actual}} - \overline{P^{\text{actual}}}\right)^2}} \tag{18}$$

where P_j^{pred}, P_j^{actual} are the j-th predicted and actual value, respectively; $\overline{P^{\text{pred}}}$, $\overline{P^{\text{actual}}}$ are the mean values of the predicted and actual values, respectively. The closer of calculated correlation coefficient to 1, the more precise of prediction results compared to the measured data, implying the strong capacity of applying the developed CGP-NN model on pore pressure prediction directly using seismic data.

4.4. Regional pressure distribution

Figs. 12 and 13 show the pressure distribution in the inline and crossline profiles over the P4 well, respectively. The Eaton method

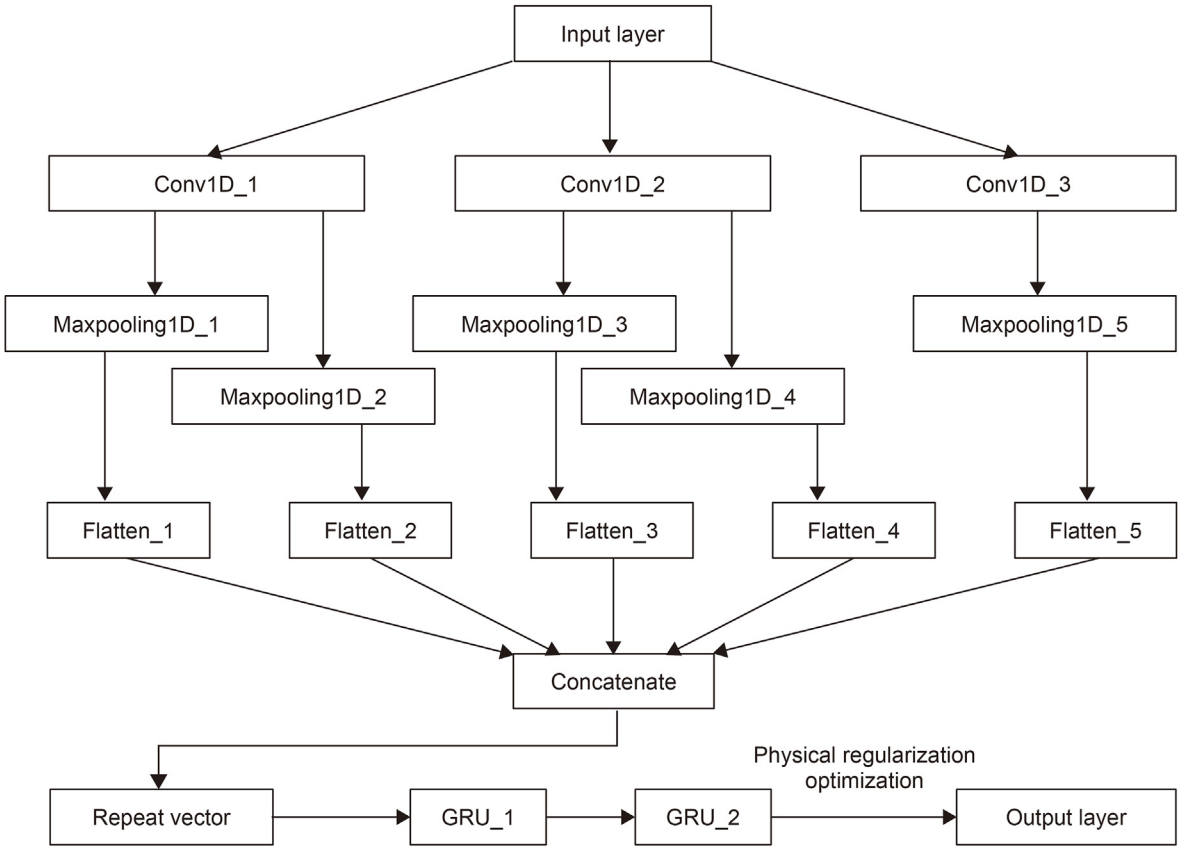

Fig. 8. The CGP-NN architecture for this research.

Table 6
CGP-NN architecture for the case study.

Type	Component	Layers	Hyper-parameter	Output shape
Encoder	Original	–	–	[None,13,1]
	PCA	–	$p = 0.95$	[None,8,1]
	Input			[None,8,1]
	1DCPP	Conv1D_1 (Input)	$f = 6, k = 2, s = 1$	[None,8,6]
		Maxpooling1d_1 (Conv1D_1)	$pool = 2$	[None,4,6]
		Flatten_1 (Maxpooling1d_1)	–	[None,24]
		Maxpooling1d_2 (Conv1D_1)	$pool = 1$	[None,8,6]
		Flatten_2 (Maxpooling1d_2)	–	[None,48]
		Conv1D_2 (Input)	$f = 6, k = 4, s = 1$	[None,5,6]
		Maxpooling1d_3 (Conv1D_2)	$pool = 2$	[None,2,6]
		Flatten_3 (Maxpooling1d_3)	–	[None,12]
		Maxpooling1d_4 (Conv1D_2)	$pool = 1$	[None,5,6]
		Flatten_4 (Maxpooling1d_4)	–	[None,30]
		Conv1D_3 (Input)	$f = 6, k = 8, s = 1$	[None,1,6]
		Maxpooling1d_5 (Conv1D_3)	$pool = 1$	[None,1,6]
		Flatten_5 (Maxpooling1d_5)	–	[None,6]
		Concatenate (Flatten_1,2,3,4,5)	–	[None,120]
		Repeat vector (Concatenate)	–	[None,3,120]
Decoder	Multilayer GRU	GRU layer_1 (Repeat vector)	$u = 128, d = 0.4$	[None,3,128]
		GRU layer_2 (GRU layer_1)	$u = 64, d = 0.2$	[None,64]
	Output	Dense (GRU layer_2)	–	[None,1]

Note: p = percentage of components left, f = numbers of filters, k = kernel size, s = strides, $pool$ = pool size, u = number of neural units, d = recurrent dropout. The total parameter numbers for the case study are 133,414.

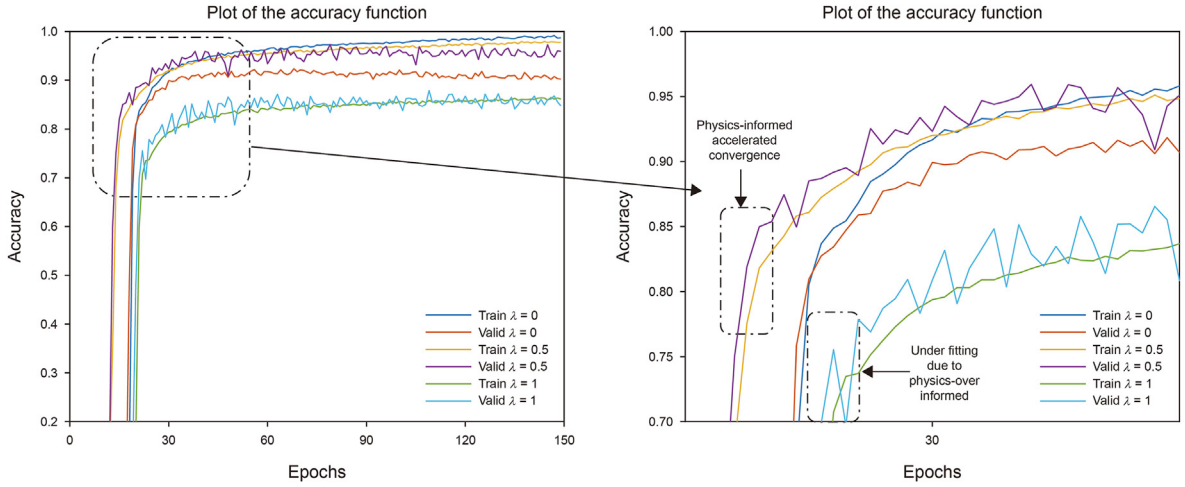

Fig. 9. The accuracy of training and validation sets with different λ

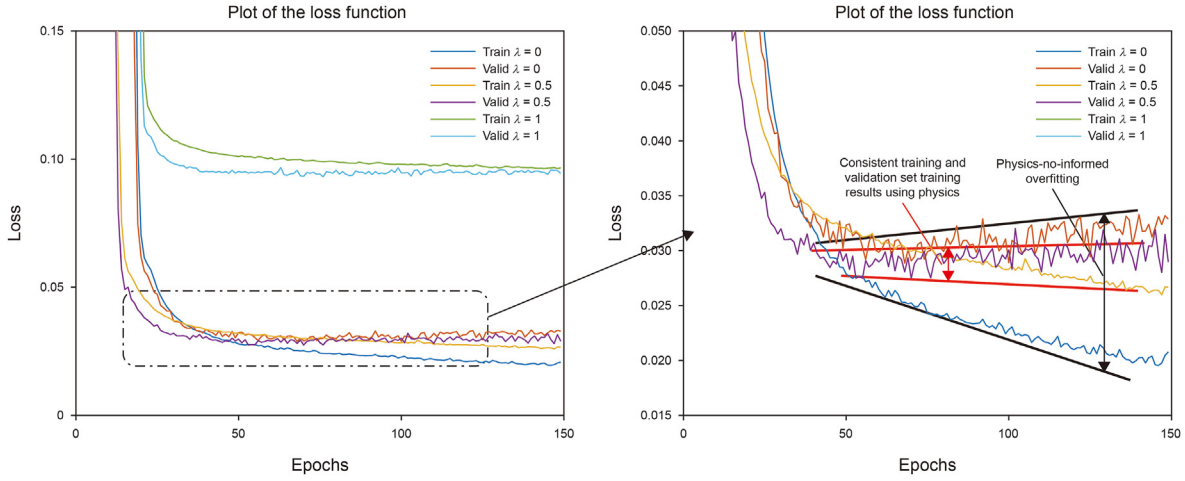

Fig. 10. The loss of training and validation sets with different λ

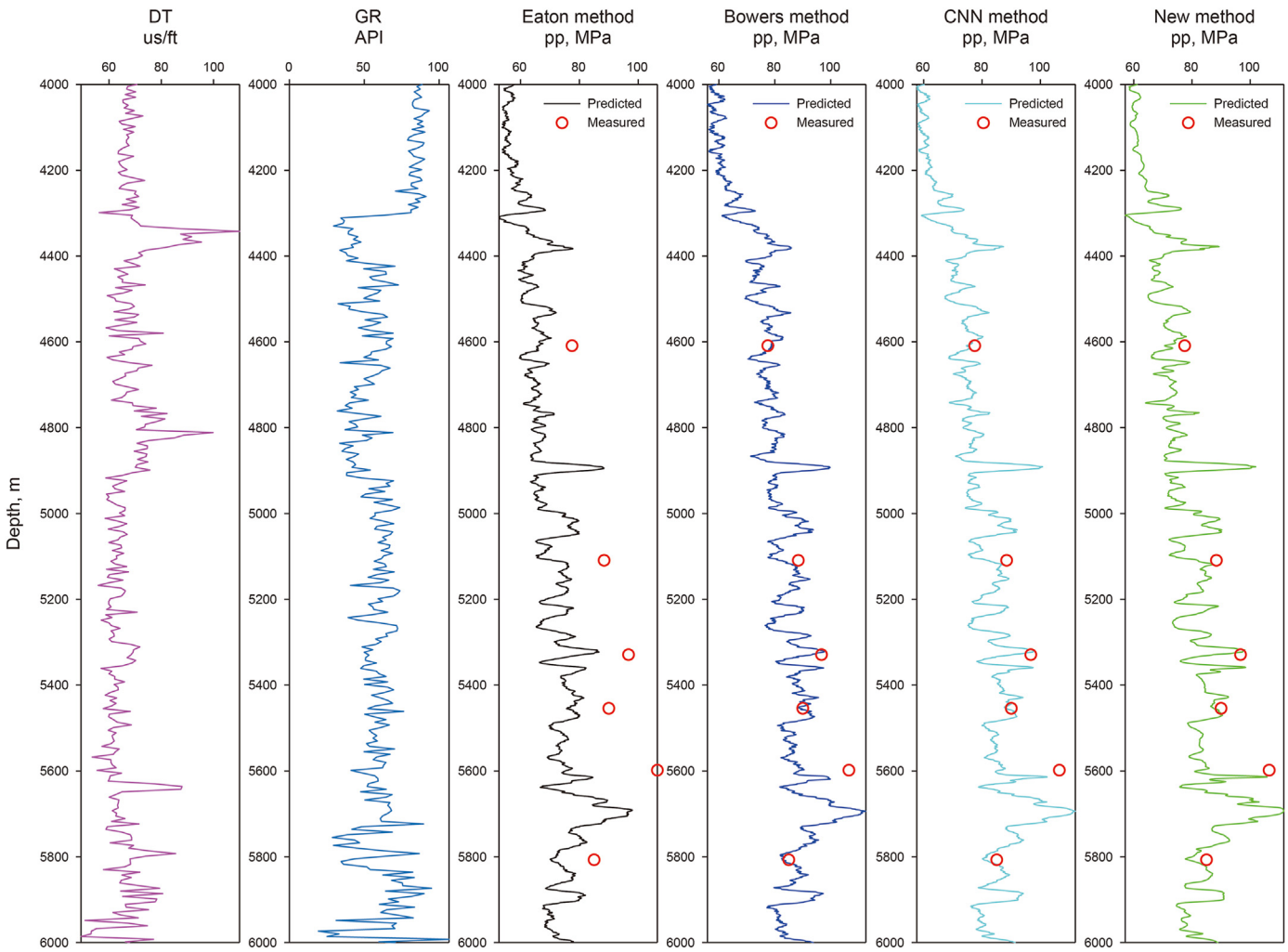

Fig. 11. Prediction results of pore pressure for well P4.

underestimates the pore pressure, as described in the literature (Bowers, 1995). The prediction results of the Eaton method seem to have better continuity, but the accuracy is low and does not match the actual situation. The actual drilling shows that the pore pressure varies greatly not only with depth but also laterally at different locations in the region. The CGP-NN method presents this true characteristic well, with discontinuities in the lateral pressure variations. In particular, the CGP-NN method accurately predicts the overflow point of the actual drilled well. Moreover, the CGP-NN method also predicts various risk points where overflow may occur during actual drilling. These results further demonstrate the generalization capability of the CGP-NN model.

4.5. Model limitation

It is worth noting that the proposed model in this work considers two theoretical models as physical constraints, implicitly assuming that the abnormal pore pressure is mainly caused by two mechanisms. In the future, the adaptive physics-informed loss function would be improved by adding physical models which represent more causal mechanisms of pore pressure.

5. Conclusions

In this study, we propose a novel adaptive physics-informed deep learning model with the name CGP-NN, which can predict the pore pressure values directly from seismic attributes data. The CGP-NN model mainly consists of a 1DCPP model, a multilayer GRU neural network and an adaptive physics-informed constraint method. First, the 1DCPP model extracts multidimensional parametric features from seismic data. Second, the corresponding pore pressure values are predicted by a multilayer GRU model with an adaptive physics-informed constraint method. To enhance the learning efficiency of the CGP-NN model and save computational resources, we propose a 1DCPP structure combining the advantages of 1DCNN and spatial pyramid pooling. To further verify the generalization and predictive ability of the developed CGP-NN model, a case study on a complex reservoir is conducted. The actual measured data demonstrated the effectiveness and generalization of the proposed model and method. Furthermore, since the adaptive physics-informed method can automatically select the most appropriate physical model as a constraint based on the error variation between the predicted and labeled values, the most appropriate physical model here may reflect the main cause of the formation pore pressure at this depth, which can be further

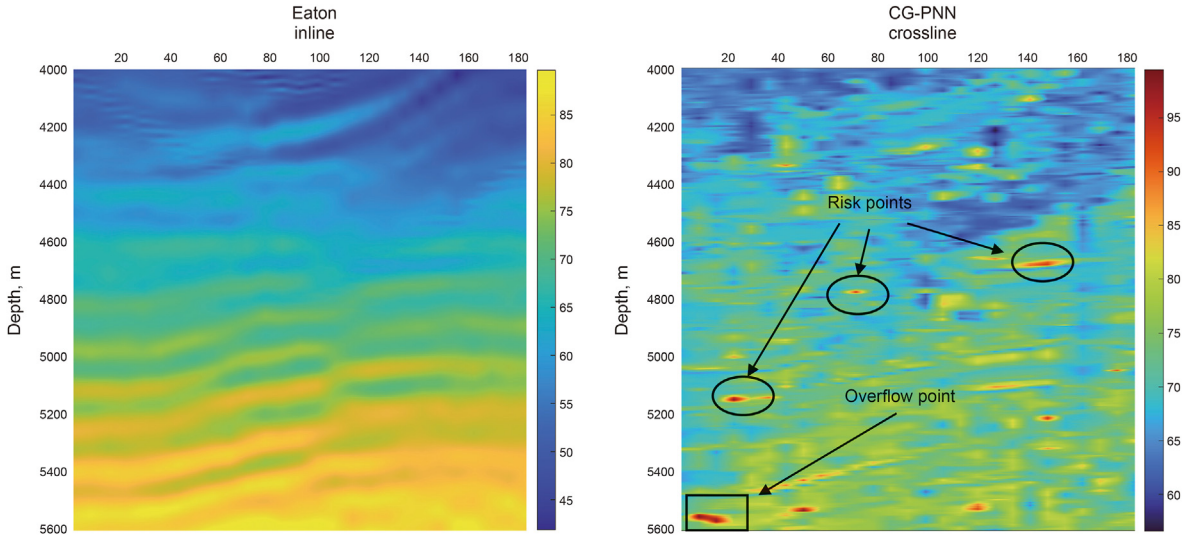

Fig. 12. Inline profile pressure distribution over P4 well.

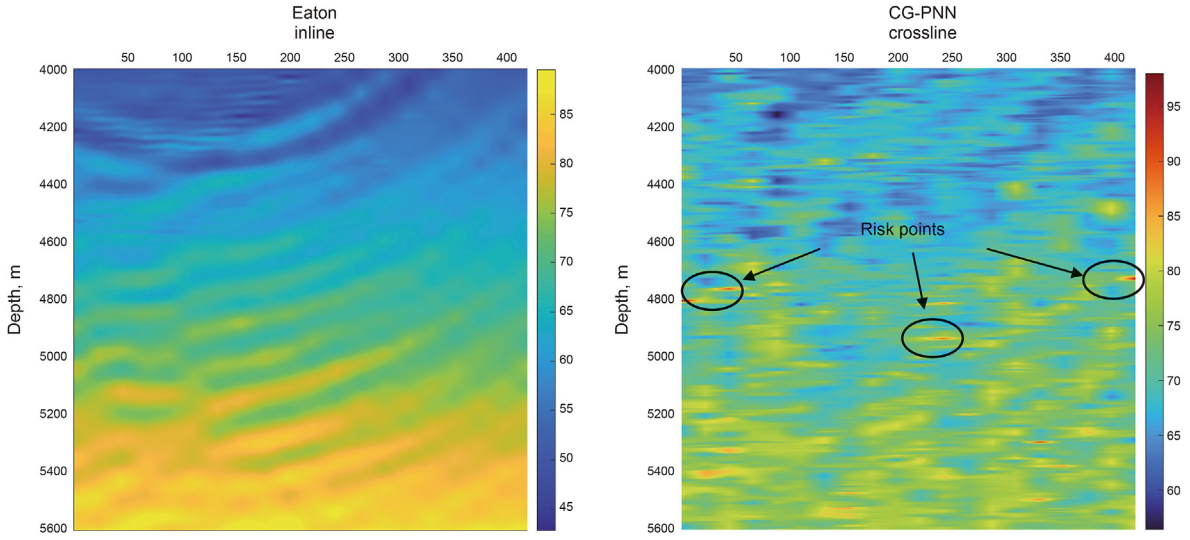

Fig. 13. Crossline profile pressure distribution over P4 well.

investigated later.

CRediT authorship contribution statement

Xin Zhang: Methodology, Writing – original draft, Validation, Visualization, Writing – review & editing. **Yun-Hu Lu:** Funding acquisition, Resources. **Yan Jin:** Conceptualization. **Mian Chen:** Supervision. **Bo Zhou:** Data curation.

Declaration of competing interest

The authors declare that they have no known competing financial interests or personal relationships that could have appeared to influence the work reported in this paper.

Acknowledgments

This research was funded by the National Natural Science Foundation of China (General Program: No. 52074314, No. U19B6003-05) and National Key Research and Development Program of China (2019YFA0708303-05).

Appendix A

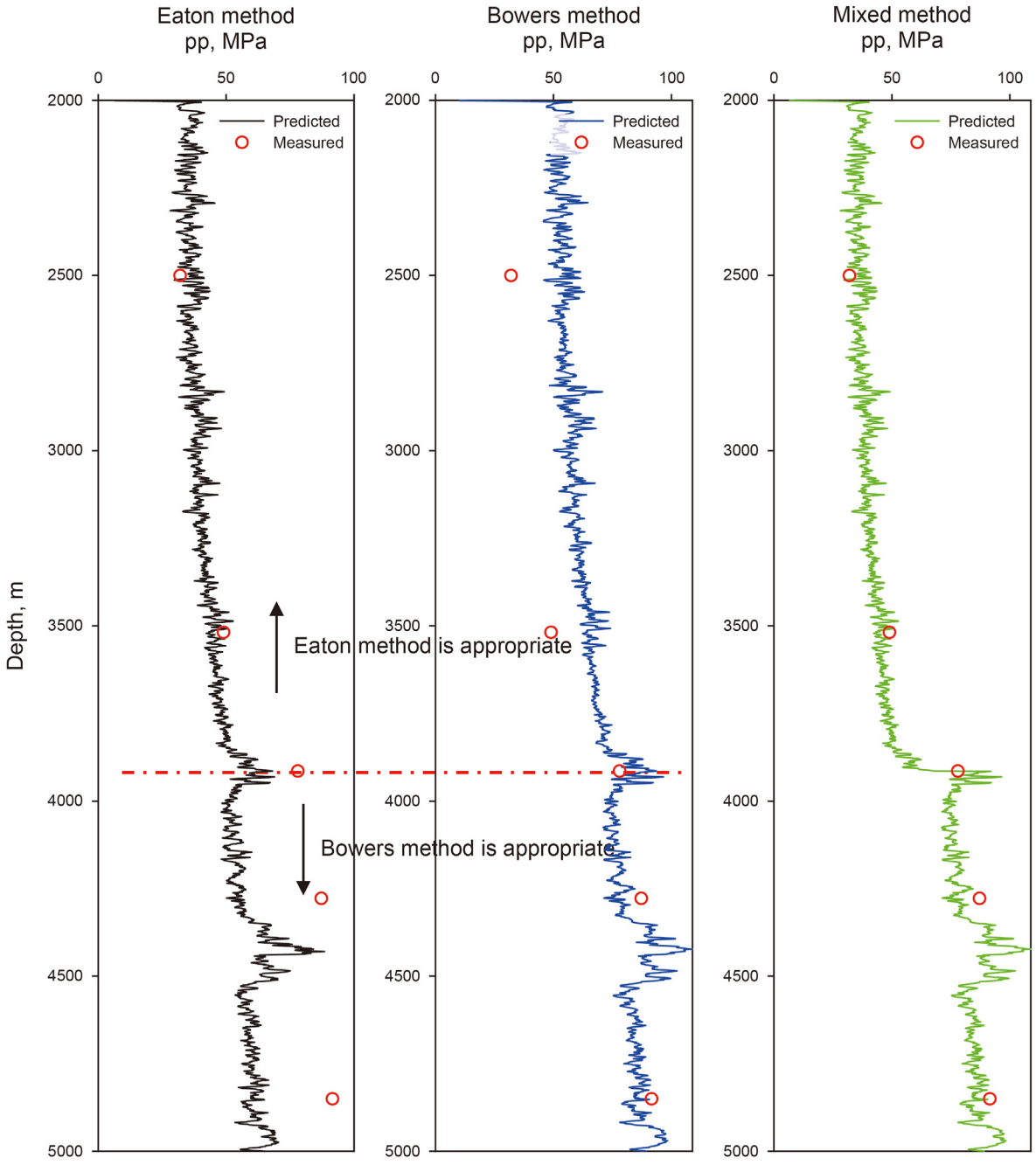

Fig. A1. Pore pressure labels for well P2.

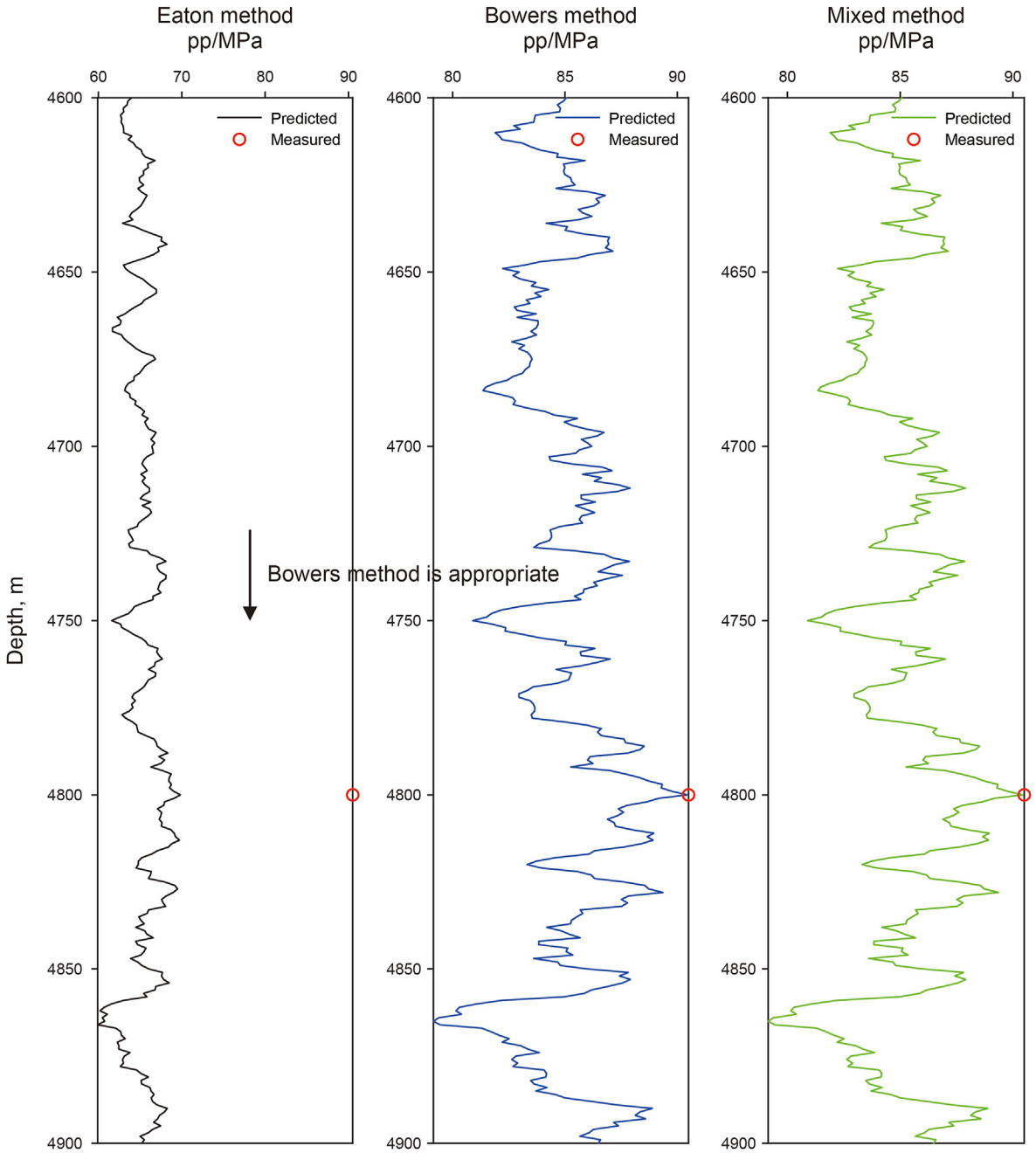

Fig. A2. Pore pressure labels for well P3.

Appendix B

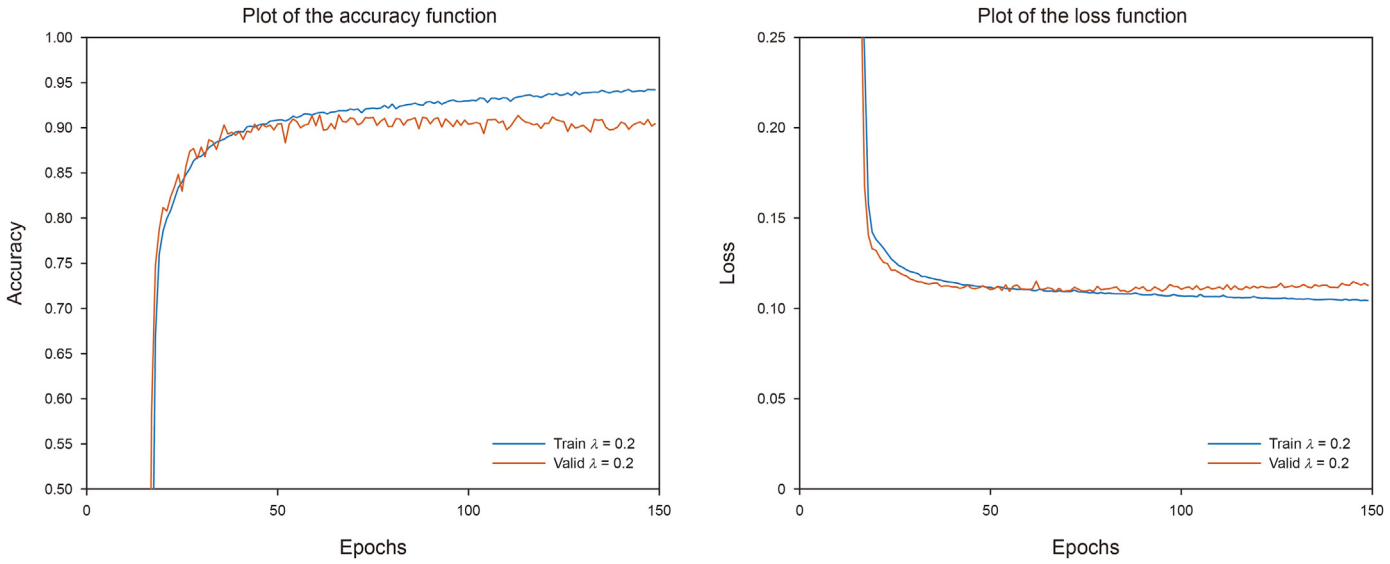

Fig. B1. The accuracy and loss of training and validation sets with $\lambda = 0.2$

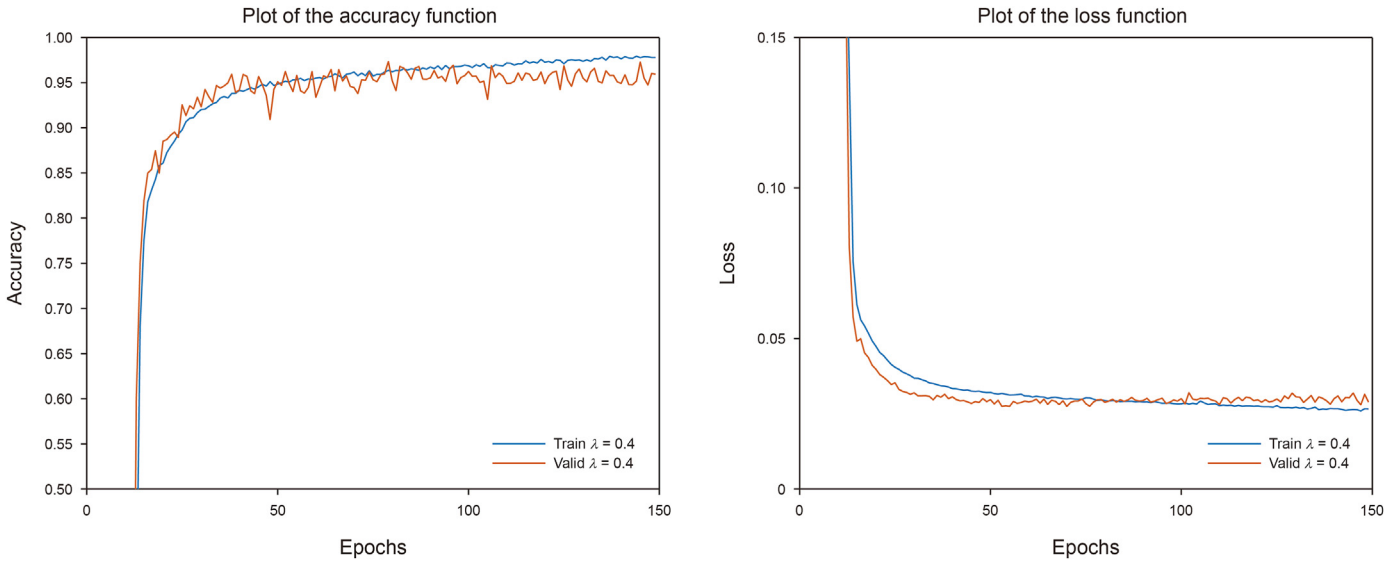

Fig. B2. The accuracy and loss of training and validation sets with $\lambda = 0.4$

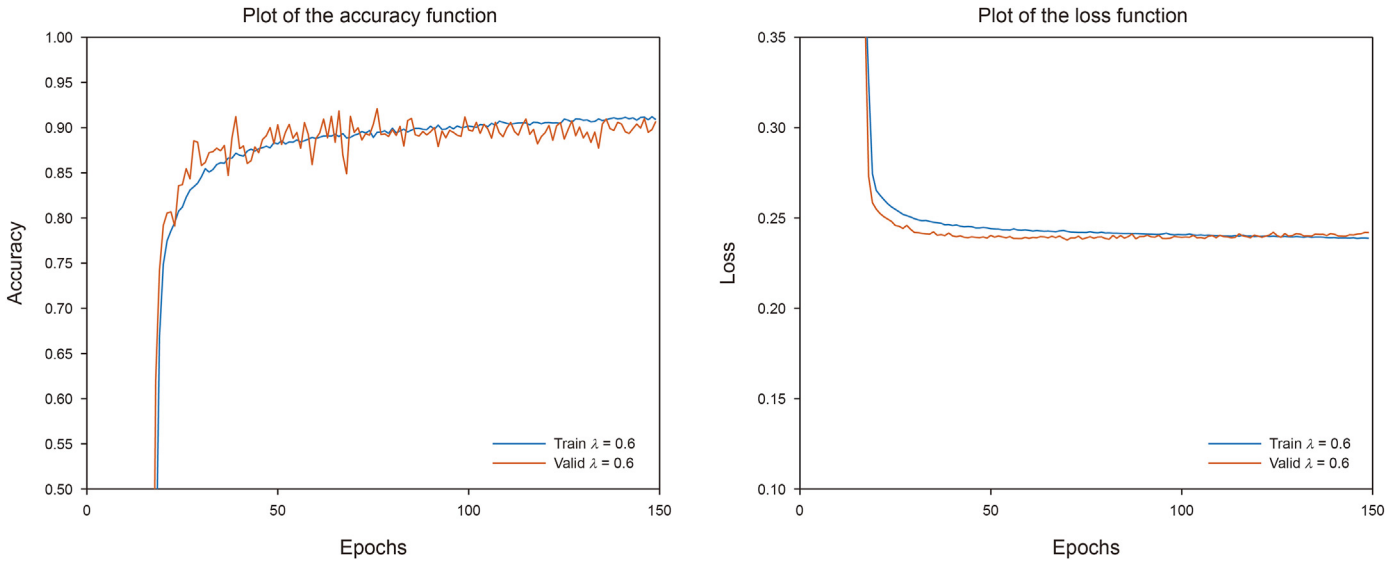

Fig. B3. The accuracy and loss of training and validation sets with $\lambda = 0.6$

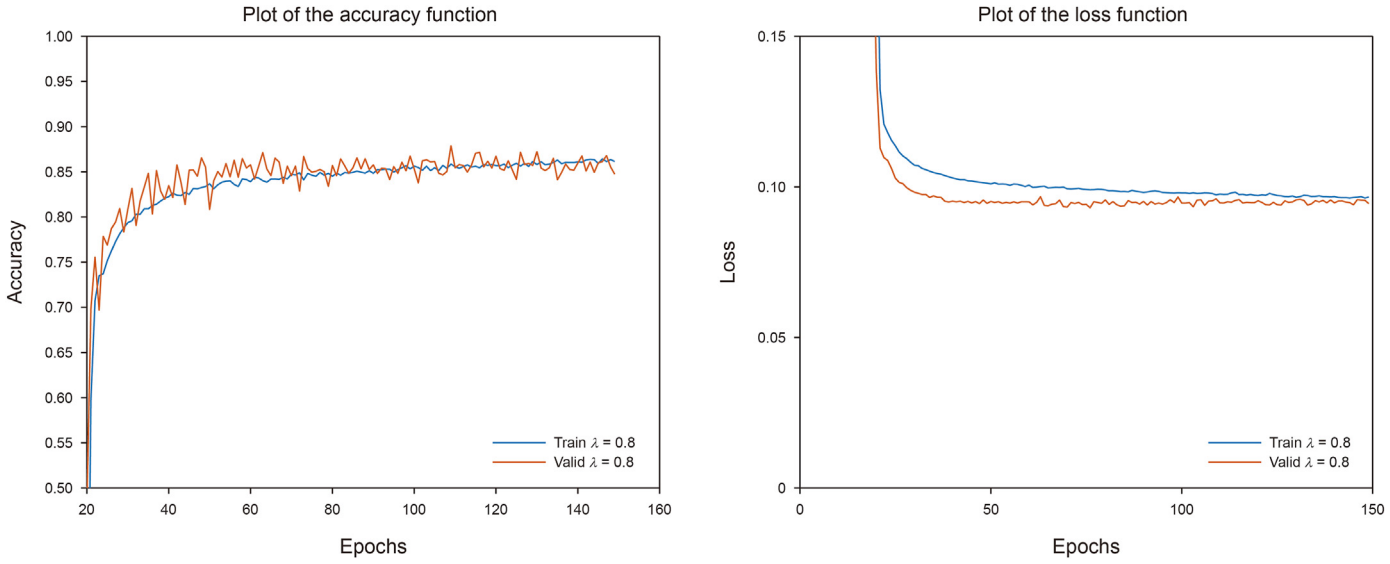

Fig. B4. The accuracy and loss of training and validation sets with $\lambda = 0.8$

References

Agrawal, V., Singh, R.K., Singh, J., et al., 2011. Role of formation pressure and sonic measurements while drilling in pre-drill well design validation and syn-drill well design optimization - case studies from deepwater, India. In: SPE Middle East Oil and Gas Show and Conference, Manama, Bahrain. https://doi.org/10.2118/142540-MS.

Boer, L., Sayers, C.M., Nagy, Z.R., et al., 2006. Pore pressure prediction using well-conditioned seismic velocities. First Break 24 (5), 43–49. https://doi.org/10.3997/1365-2397.2006012.

Bowers, G.L., 1995. Pore pressure estimation from velocity data: accounting for overpressure mechanisms besides undercompaction. SPE Drill. Complet. 10 (2), 89–95. https://doi.org/10.2118/27488-PA.

Bowers, G.L., 2001. Determining an appropriate pore-pressure estimation strategy. In: Offshore Technology Conference, Houston, Texas. https://doi.org/10.4043/13042-MS .

Chen, F.B., Zong, Z.Y., 2022. PP-wave reflection coefficient in stress-induced anisotropic media and amplitude variation with incident angle and azimuth inversion. Geophysics 87 (6), C155–C172. https://doi.org/10.1190/geo2021-0706.1.

Chen, F.B., Zong, Z.Y., Yin, X.Y., 2023. Monitoring the change in horizontal stress with multi-wave time-lapse seismic response based on nonlinear elasticity theory. Petrol. Sci. 20 (2), 815–826. https://doi.org/10.1016/j.petsci.2022.09.022.

Cho, K., Van Merrienboer, B., Bahdanau, D., et al., 2014. On the properties of neural machine translation: encoder-decoder approaches. https://doi.org/10.48550/arXiv.1409.1259.

Chung, J., Gulcehre, C., Cho, K., et al., 2014. Empirical evaluation of gated recurrent neural networks on sequence modeling. https://doi.org/10.48550/arXiv.1412.3555.

Cibin, P., 1999. What seismic velocity field for pore pressure prediction. SEG Tech. Progr. Expand. Abstr. 23 (1). https://doi.org/10.1190/1.1851132.

Dong, C., Loy, C.C., He, K., et al., 2016. Image super-resolution using deep convolutional networks. IEEE Trans. Pattern Anal. Mach. Intell. 38 (2), 295–307. https://doi.org/10.1109/TPAMI.2015.2439281.

Dutta, N., 2002. Geopressure prediction using seismic data: current status and the road ahead. Geophysics 67 (6), 2012–2041.

Eaton, B.A., 1975. The equation for geopressure prediction from well logs. In: The Society of Petroleum Engineers of AIME, Dallas, Texas. https://doi.org/10.2118/5544-MS.

Farsi, M., Mohamadian, N., Ghorbani, H., et al., 2021. Predicting formation pore-pressure from well-log data with hybrid machine-learning optimization algorithms. Nat. Resour. Res. 30, 3455–3481. https://doi.org/10.1007/s11053-021-09852-2.

Gao, Y., Chen, M., Jiang, H., 2021. Influence of unconnected pores on effective stress in porous geomaterials: theory and case study in unconventional oil and gas reservoirs. J. Nat. Gas Sci. Eng. 88, 103787.

Gutierrez, M.A., Braunsdorf, N.R., Couzens, B.A., 2006. Calibration and ranking of pore-pressure prediction models. Lead. Edge 25 (12), 1516–1523.

He, K., Zhang, X., Ren, S., et al., 2015. Spatial pyramid pooling in deep convolutional networks for visual recognition. In: IEEE Transactions on Pattern Analysis and Machine Intelligence, pp. 1904–1916.

Hochreiter, S., Schmidhuber, J., 1997. Long short-term memory. Neural Comput. 9 (8), 1735–1780.

Hottmann, C.E., Johnson, R.K., 1965. Estimation of formation pressures from log-derived shale properties. J. Petrol. Technol. 17 (6), 717–722.

Huang, G., Liu, Z., van der Maaten, L., et al., 2017. Densely connected convolutional networks. In: 30th IEEE Conference on Computer Vision and Pattern Recognition, New York, pp. 2261–2269.

Huang, H., Li, J., Yang, H., et al., 2022. Research on prediction methods of formation pore pressure based on machine learning. Energy Sci. Eng. 10 (6), 1886–1901. https://doi.org/10.1002/ese3.1112.

Jin, J., Jin, Y., Lu, Y., et al., 2022. Image processing and machine learning based cavings characterization and classification. J. Petrol. Sci. Eng. 208, 109525. https://doi.org/10.1016/j.petrol.2021.109525.

Keshavarzi, R., Jahanbakhshi, R., 2013. Real-time prediction of pore pressure gradient through an artificial intelligence approach: a case study from one of middle east oil fields. Euro. J. Environ. Civil Eng. 17 (8), 675–686. https://doi.org/10.1080/19648189.2013.811614.

Kim, Y., 2014. Convolutional neural networks for sentence classification. https://doi.org/10.48550/arXiv.1408.5882.

LeCun, Y., Bengio, Y., Hinton, G., 2015. Deep learning. Nature 521 (7553), 436–444. https://doi.org/10.1038/nature14539.

Li, Q.F., Fu, J.H., Chi, P., et al., 2023. A deep learning approach for abnormal pore pressure prediction based on multivariate time series of kick. Geoenergy Sci. Eng. 226, 211715. https://doi.org/10.1016/j.geoen.2023.211715.

Lopez, J.L., Rappold, P.M., Ugueto, G.A., et al., 2004. Integrated shared earth model: 3D pore-pressure prediction and uncertainty analysis. Lead. Edge 23 (1), 52–59.

Matinkia, M., Amraeiniya, A., Behboud, M.M., et al., 2022. A novel approach to pore pressure modeling based on conventional well logs using convolutional neural network. J. Petrol. Sci. Eng. 211, 110156. https://doi.org/10.1016/j.petrol.2022.110156.

Najibi, A.R., Ghafoori, M., Lashkaripour, G.R., et al., 2017. Reservoir geomechanical modeling: in-situ stress, pore pressure, and mud design. J. Petrol. Sci. Eng. 151, 31–39. https://doi.org/10.1016/j.petrol.2017.01.045.

Opara, A.I., Onuoha, K.M., 2009. Pre-drill pore pressure prediction from 3-D seismic data in parts of the onshore Niger delta basin. In: SPE International Technical Conference and Exhibition in Abuja, Abuja, Nigeria. https://doi.org/10.2118/128354-ms.

Oprea, S., Martinez-Gonzalez, P., Garcia-Garcia, A., et al., 2022. A review on deep learning techniques for video prediction. IEEE Trans. Pattern Anal. Mach. Intell. 44 (6), 2806–2826. https://doi.org/10.1109/TPAMI.2020.3045007.

Oughton, R.H., Wooff, D.A., Hobbs, R.W., et al., 2018. A sequential dynamic bayesian network for pore-pressure estimation with uncertainty quantification. Geophysics 83 (2), D27–D39. https://doi.org/10.1190/geo2016-0566.1.

Sayers, C.M., Johnson, G.M., Denyer, G., 2002. Predrill pore-pressure prediction using seismic data. Geophysics 67 (4), 1286–1292. https://doi.org/10.1190/1.1500391.

Subrahmanyam, D., Rao, P.H., 2008. Seismic attributes-a review. In: 7th International Conference and Exposition on Petroleum Geophysics. Hyderabad.

Szegedy, C., Liu, W., Jia, Y., et al., 2015. Going deeper with convolutions. In: IEEE Conference on Computer Vision and Pattern Recognition, New York. https://doi.org/10.1109/cvpr.2015.7298594.

Tjur, T., 2009. Coefficients of determination in logistic regression models-a new proposal: the coefficient of discrimination. Am. Statistician 63 (4), 366–372. https://doi.org/10.1198/tast.2009.08210.

Wang, Z., Wang, R., 2015. Pore pressure prediction using geophysical methods in carbonate reservoirs: current status, challenges and way ahead. J. Nat. Gas Sci. Eng. 27, 986–993. https://doi.org/10.1016/j.jngse.2015.09.032.

Weinzierl, W., Wiese, B., 2021. Deep learning a poroelastic rock-physics model for pressure and saturation discrimination. Geophysics 86 (1), MR53–MR66.

Wessling, S., Bartetzko, A., Tesch, P., 2013. Quantification of uncertainty in a multistage/multiparameter modeling workflow: pore pressure from geophysical well logs. Geophysics 78 (3), WB101–WB112.

Yang, J., Zhang, D., Frangi, A.F., et al., 2004. Two-dimensional PCA: a new approach to appearance-based face representation and recognition. IEEE Trans. Pattern Anal. Mach. Intell. 26 (1), 131–137.

Ye, M., Shen, J., Lin, G., et al., 2022. Deep learning for person re-identification: a survey and outlook. IEEE Trans. Pattern Anal. Mach. Intell. 44 (6), 2872–2893. https://doi.org/10.1109/TPAMI.2021.3054775.

Yu, F., Jin, Y., Chen, K.P., et al., 2014. Pore-pressure prediction in carbonate rock using wavelet transformation. Geophysics 79 (4), D243–D252. https://doi.org/10.1190/geo2013-0277.1.

Zhang, J., 2011. Pore pressure prediction from well logs: methods, modifications, and new approaches. Earth Sci. Rev. 108 (1–2), 50–63. https://doi.org/10.1016/j.earscirev.2011.06.001.

Zhang, J., Yin, S., 2017. Real-time pore pressure detection: indicators and improved methods. Geofluids 2017, 3179617. https://doi.org/10.1155/2017/3179617.

Zhang, Z., Sun, B., Wang, Z., et al., 2022. Formation pressure inversion method based on multisource information. SPE J. 27 (2), 1287–1303. https://doi.org/10.2118/209206-PA.

Zhao, J., 2019. Speech emotion recognition using deep 1D and 2D CNN LSTM networks. Biomed. Signal Process Control 47, 312–323. https://doi.org/10.1016/j.bspc.2018.08.035.